Eur. Phys. J. D **36**, 271–280 (2005)
DOI: 10.1140/epjd/e2005-00244-0

THE EUROPEAN PHYSICAL JOURNAL D

Vibrational inelastic electron-H_2 scattering revisited: numerically converged coupled channels space frame calculations with model interactions

S. Telega[a] and F.A. Gianturco[b]

Department of Chemistry, University of Rome "La Sapienza" and INFM, Piazzale A. Moro 5, 00185 Rome, Italy

Received 14 March 2005/ Received in final form 31 May 2005
Published online 30 August 2005 –

Abstract. The collisional excitation of the lower vibrational levels of $H_2(^1\Sigma_g^+)$ molecules by low-energy electron impact is computed using an empirical model potential and by solving the coupled-channels scattering equations within a space-fixed (SF) frame of reference formulation. Numerically converged partial, integral inelastic and elastic cross-sections are obtained from what is an essentially exact treatment of the dynamics and the results are compared with measurements and with earlier calculations on the same system. The usefulness of the SF method for handling excitation processes at near-threshold collision energies is discussed and analyzed through the calculations of collisional superelastic partial cross-sections down to 10^{-2} meV of collision energy.

PACS. 34.80.Bm Elastic scattering of electrons by atoms and molecules – 34.80.-i Electron scattering

1 Introduction

The study of the low-energy scattering of electron beams off gaseous molecules provides a great variety of experimental outcomes that turn out to be of relevance in a correspondingly broad range of chemistry and physics areas of study, from astrophysical processes initiated by photoelectrons in the interstellar medium to chemical reactions that follow ionization by discharge in the gaseous molecular mixture [1–3]. Thus, to be able to establish a reliable set of scattering observables for an increasingly broader range of molecular targets which are of relevance in so many areas has indeed provided the motivation for a great deal of experimental work [4,5].

The corresponding theoretical analysis of such observables, either along series of similar molecules to establish possible patterns of behaviour, or focussing on a particular target gas to evaluate several types of inelastic cross-sections, integral and differential, within a specific medium, has been challenged to produce a similarly broad range of data for a great variety of molecular gases and to achieve in the evaluation of the relevant scattering observables a comparable level of accuracy and reliability [6].

A case in point is provided by the analysis of the very impressive set of data which have been gathered about molecular hydrogen, one of the most abundant molecules in our planetary system and in the interstellar medium. Apart from the extensive review of the existing data published a while ago [4], there has been a more specific analysis of such data on H_2 [7] dealing chiefly with excitation cross-sections, while a set of recommended cross-sections for elastic and inelastic processes has been given in reference [8]. On the theoretical side, a recent review by Morrison et al. [9] provides an extensive summary of the comparison between experiments and theory in the low-energy regimes, focussing on rovibrational excitation processes. Finally, a very recent presentation and critical comparison of all the existing data for molecular hydrogen, together with many other diatomic molecules, has been excellently compiled by Brunger et al. [12] just a couple of years ago.

Further progress of the research in recent years has been provided by the study of very-low energy electron collisions with gaseous molecules [10,11], where the corresponding theoretical analysis of the dynamics inevitably requires one to treat correctly the coupling between internal rovibrational motion and that of the impinging electron [6], i.e. to proceed beyond the more approximate Body-Fixed (BF) analysis of the energy transfer processes that is known to be realistic at collision energies well above the corresponding thresholds [9]. The full, coupled channel treatments of the above processes, however, poses serious convergence problems on the numerical side and has rarely been carried out explicitly to full convergence by the earlier computational studies [1,2]

The object of the present study is therefore that of revisiting what has been found for the vibrationally inelastic processes at low scattering energies in the case of e^-–H_2

[a] *Present address:* Faculty of Applied Physics and Mathematics, Technical University of Gdańsk, 80952 Gdańsk, Poland.
[b] e-mail: fa.gianturco@caspur.it

collisions in the gas phase and to carry out a numerically converged study of the lower vibrationally inelastic, rotationally summed, partial integral cross-sections by solving the scattering quantum problem exactly within a space-fixed (SF) reference frame representation of the corresponding Coupled Channels (CC) equations. In particular, we intend to employ a recently implemented form of the above equations [13] where use is made of a modified formulation of the Variable Phase (VP) treatment of the dynamics [14] within the multichannel situation of a molecular system.

What we report in the following, therefore, is not intended to provide an exhaustive comparison with all the many results on H_2 already obtained through the enormous literature of the last 30 years, but rather a proof-of-principle on the use of a converged SF treatment with model interaction to obtain, at the energies where experiments and calculations already exist, good agreement with those findings. Such an agreement should therefore bode well for the intended extensions of the present method down to energies very close to rovibrational thresholds (where the SF approach becomes indispensable) which we shall test here only in a preliminary way while further extensions to other systems at lower energies will be presented elsewhere. In the following section, we therefore summarize first our theoretical approach and further describe more in detail our numerical implementation of it. Section 3 reports and discusses the present results while Section 4 summarizes our conclusions.

2 The theoretical formulation

2.1 The quantum dynamics

In the case of the small distorsions which are induced into the target by the impinging particle, the total scattering wavefunction can be expanded in terms of asymptotic target rotational and vibrational eigenfunctions

$$\mathcal{H}_{mol}(\mathbf{R})\chi_\nu(R)Y_{jmj}(\hat{\mathbf{R}}) = [\varepsilon_\nu + \frac{\hbar^2}{2I}j(j+1)]\chi_\nu(R)Y_{jmj}(\hat{\mathbf{R}}) \quad (1)$$

ε_ν being the vibrational eigenvalue, I the isolated molecule moment of inertia [13] ($\hat{R}$) the space orientation of the molecular bond and R the varying intermolecular distance. Hence, the total scattering wavefunction is given as

$$\Psi_n(E, \mathbf{r}_e, \mathbf{R}) = \sum_f u_{i\to f}(\mathbf{r}_e, E)\chi_f(R)Y_f(\hat{\mathbf{R}}) \quad (2)$$

where $|f\rangle$ denotes the $|\nu' j' m_{j'}\rangle$ final states of the vibrating molecule that are involved in the expansion and the $u_{i\to f}(\mathbf{r}_e, E)$ are the channel components of the scattering wavefunction which have to be determined by solving the usual Schrödinger equation subject to its scattering boundary conditions, with $\mathbf{r}_e$ being the scattered electron vector position from the molecular center of mass (c.o.m.)

$$u_{i\to f}(\mathbf{r}_e) \to \delta_{if}h^{(-)}(\mathbf{r}_e) - S_{if}h^{(+)}(\mathbf{r}_e) \quad \text{as } (\mathbf{r}_e)\sim\infty \quad (3)$$

here $h^{(\pm)}(\mathbf{r}_e)$ is a pair or linearly independent free partial solutions defined as

$$h_{if}^{(\pm)} \sim \delta_{if}k_i^{-1/2}\exp\left[i(k_i r \pm l_i\pi/2)\right]. \quad (4)$$

When they are chosen to be appropriate Riccati-Hankel functions, then the S_{if} coefficients become the elements of the reduced scattering matrix, often additionally labelled by the total angular momentum of the system: $\mathbf{J} = \mathbf{j} + \mathbf{l}$, the latter $\mathbf{l}$ being the continuum electron partial-wave component. Usually, one expects that the numerically converged scattering observables can be obtained by retaining only a limited number of discrete, asymptotic target states in the expansion (2). The $u_{i\to f}$ are therefore expanded in products of total angular momentum eigenfunctions and of radial functions $\varphi^J_{\lambda\lambda'}(E, r_e)$, where J is the magnitude of the total angular momentum and, $\lambda' = (j', l')$. The radial functions are in turn solutions of the familiar set of coupled, second order homogeneous differential equations (in the case of local interactions) [13,14]

$$\left[\frac{d^2}{dr_e^2}\mathbf{I}^2 - \frac{1}{r_e^2}\mathbf{l}^2 + \mathbf{K}_\nu^2\right]\mathbf{\Phi}^J_\nu(E, r_e) = \sum_{\nu'}\mathbf{U}^J_{\nu\nu'}\mathbf{\Phi}^J_{\nu'}(E, r_e) \quad (5)$$

where $\mathbf{I}$ is the unit matrix, $\mathbf{\Phi}^J$ is the matrix of radial functions and

$$(\mathbf{l}^2)_{\lambda\lambda'} = l'(l'+1)\delta_{\lambda\lambda'} \quad (6)$$

$$(\mathbf{K}^2_\nu)_{\lambda\lambda'} = k^2_{j\nu}\delta_{\lambda\lambda'} = (2/\hbar^2)(E - E_{j\nu})\delta_{\lambda\lambda'} \quad (7)$$

$$(\mathbf{U}^J_{\nu\nu'}(r_e))_{\lambda\lambda'} = \sum_L f_L(lj; l'j'; J)\langle\chi_\nu|V_L(r_e)(R)|\chi_{\nu'}\rangle \quad (8)$$

where the $f_L(lj; l'j'; J)$ are the well-known, real coefficients of Percival and Seaton [6,9] and the coupling between the asymptotic (diabatic) target states is given by the radial matrix elements of equation (8), which we shall discuss in detail in the next section. As is well-known, the direct coupling between rotational levels will be controlled by the largest multipolar coupling V_L included in equation (8). The corresponding vibrational couplings will involve the strength of the V_L terms over the internuclear variable and convoluted over several (ν, ν') vibrational asymptotic states and gives rise to diagonal and off-diagonal coupling terms: $V_L^{\nu\nu'}(r_e)$ in equation (8), where the $\chi_\nu(R)$ are the target asymptotic vibrational wavefunctions.

The number of channels to be included in the expansion for equation (4) obviously depends on the system and on the collision energy. Furthermore, for each selected collision energy it also depends on the region of interaction that is being sampled during the search for the channel eigenfunctions. In the short-range regions, which correspond to the strongest interactions, one should include all those channels which become locally open because of

the attractive features of the given interaction (and which would be asymptotically closed, at least some of them). Their number could be very large in the present situations where the Coulomb interaction is the strongest over the nuclear cusp regions. On the other hand, in the weaker asymptotic region for $r_e \sim \infty$, only a few of the open channels will be needed. In between these two extreme situations there is a region of interaction where the closed channels change their importance with distance and therefore could be varied in number accordingly. Just to treat such demanding interaction forces during an exact quantum dynamics, we have recently developed [13] a suitable numerical algorithm that judiciously performs the controls along the radial evaluation process and modifies the size of the relevant S-matrix. We have called it the Modified Variable Phase Approximation (MVPA) and have employed it in the present case to solve the set of coupled equations (4). The gain in the computational effort can be of about two orders of magnitude with respect to more conventional methods [13].

Typically, for numerical convergence we needed to use the full coupling from about 10^{-5} Å (the initial integration point) out to 4.0 Å, then we could gradually reduce the K-matrix size out to 400 Å over a step of 0.002 Å for a total of 5000 steps. The total angular momentum values went up to 3 while the target rotational basis was extended up to 16: the rotational constant of the former target was taken to be 60.853 cm^{-1}. The multipolar coefficients of the potential expansion went up to $\lambda_{max} = 18$ for the hydrogen target and the corresponding partial-wave angular momenta for the scattered electron therefore went up to $l_{max} = 21$. The number of vibrational levels included in the expansion was of five levels up to $\nu_{max} = 4$. The integration over the internuclear coordinate of the coupling matrix elements of equation (8) run from $R_{min} = 0.5a_o$ up to $R_{max} = 3.6a_o$, covering a range of 6 vibrational levels; the latters were obtained by numerical integration over the potential energy curve using the program level [15]. The above parameters produce convergence of the S-matrix elements of the order of about 10^{-3}–10^{-4} with respect to further extensions of the CC parameters indicated above. To our knowledge, such stringent convergence tests on SF inelastic observables for the present system has not been reported before. We will show in a later section a set of actual examples for such convergence tests.

2.2 The electron-molecule interaction

2.2.1 The single center expansion

Resonant and non-resonant low-energy scattering of electrons from polyatomic targets can be studied theoretically (and computationally) at various levels of sophistication for the description of: (i) the electronuclear structure of the target molecule, (ii) the interaction forces between the bound particles and the impinging electron and (iii) the dynamical formulation of the quantum scattering equations.

We employ an ab initio, parameter-free approach which starts with the target nuclei varying their internuclear distance over a preselected range of values (see preceding section). Furthermore, the target of N-electrons is in a specific molecular electronic state (which, for the present purpose, is taken to be the ground state) and is described using the Hartree-Fock, Self-Consistent Field (SCF) approximation via the Single-Determinant (SD) description of its $N/2$ occupied Molecular Orbitals (MOs). In our implementation of the scattering equations the occupied MOs of the targets are again expanded on a set of symmetry-adapted angular functions with their corresponding radial coefficients represented on a numerical grid [16]. In this approach, any arbitrary three-dimensional function describing a given electron, either one of the N bound electrons or the scattering electron, is expanded around a single-center (SCE) usually taken to be the c.o.m. of the global $(N + 1)$ electron molecular structure

$$F^{p\mu}(r, \hat{\mathbf{r}}|\mathbf{R}) = \sum_{l,h} r^{-1} f_{lh}^{p\mu}(r|\mathbf{R}) X_{lh}^{p\mu}(\hat{\mathbf{r}}). \tag{9}$$

The above SCE representation refers here to the μth element of the pth irreducible representation (IR) of the point group of the molecule at the nuclear geometry $\mathbf{R}$. The angular functions $X_{lh}^{p\mu}(\hat{\mathbf{r}})$ are symmetry adapted angular functions given by proper combination of spherical harmonics $Y_{lm}(\hat{\mathbf{r}})$

$$X_{lh}^{p\mu}(\hat{\mathbf{r}}) = \sum_{m} b_{lmh}^{p\mu} Y_{lm}(\hat{\mathbf{r}}). \tag{10}$$

The details about the computation of the $b_{lmh}^{p\mu}$ have been given by us before and will not be repeated here [17,18].

2.2.2 The anisotropic potential

For a target which has a closed-shell electronic structure with n_{occ} doubly occupied orbitals φ_i, its interaction with a scattering electron as first given by its Exact Static+Exchange contributions

$$V_{ESE}(\mathbf{r}) = \sum_{k=1}^{M} \frac{-Z_k}{|\mathbf{r} - \mathbf{R}_k|} + \sum_{i=1}^{n_{occ}} (2\hat{J}_i - \hat{K}_i) \tag{11}$$

where $\hat{J}_i$ and $\hat{K}_i$ are the usual local static potential and the non-local exchange potential operators, respectively. The index k labels one of the M nuclei located at the coordinate $\mathbf{R}_k$ in the c.o.m., molecular frame of reference (MF). Electron-molecule scattering cross-sections (integral and differential) which are computed using only the V_{ESE} potential show in general limited agreement with experimental data of elastic scattering and become even worse when dealing with resonant scattering. The reason lies in its lack of description of the target response, i.e. of the effects of long-range polarization of the bound electrons by the charged projectile and of the short-range dynamical correlation between the latter and the molecular electrons.

At higher collision energies this is reflected in the fact that no electronically inelastic processes can be treated at the ESE level of interaction. At the lower energy, of more direct interest in the present study, the lack of inclusion of the target response leads to the neglect of important polarization effects which then causes the wrong energy behaviour and magnitude of the elastic cross-sections and which further significantly shifts positions and widths of the shape resonances, if existing. For the case of polyatomic targets we have developed over the years a model, nonempirical treatment of both exchange and correlation forces [17–22] which markedly reduces the computational effort while however producing very good accord with available experimental cross-sections [19–23]. It is that description of the full electron-molecule interaction which we adopt in the present study of a simple diatomic target.

To further include in the electron-molecule potential the long-range polarization terms and the short-range dynamical correlation effects, we have implemented a local energy-independent model potential, $V_{ecp}(\mathbf{r})$, discussed in our earlier work [23]. Briefly, the V_{ecp} potential contains a short-range correlation contribution, V_{corr}, which is smoothly connected to a long-range polarization contribution, V_{pol}, both terms being specific for electron projectiles. The short-range term is obtained by finding where the two radial coefficients for $l = 0$ first intersect. This has been, in fact, what we found in many cases to be the more effective choice in terms of the global smoothness of the total potential [23]. Hence, one writes down the full potential as

$$V_{ecp}(\mathbf{r}_e|R) = \begin{cases} V_{corr}(\mathbf{r}_e|R) & r_e \le r_{match} \\ V_{pol}(\mathbf{r}_e|R) + \sum_{lm} C_{lm}\, r^{-\lambda}\, Y_{lm}(\hat{\mathbf{r}}_e) & r_e > r_{match} \end{cases} \quad (12)$$

The C_{lm} coefficients have been determined to make the potential continuous at r_{match} and the exponent λ is a function of l such that: $\lambda(l) = 6, 5, 6$ for $l = 0, 1, 2$ and $\lambda(l) = l + 2$ for $l \ge 3$. The matching functions are chosen in a way in which each term added to V_{pol} after r_{match} has the same functional form of the first term neglected in the perturbation expansion of V_{pol}. The present values of r_{match} for $l = 0$ are around $4.0a_o$ for H_2 and vary depending on the internuclear coordinate values. This interaction now corresponds to solving our the scattering equations using Static-Exchange-Correlation-Polarization (SECP) potentials.

The polarization term contains the spherical and nonspherical parts of the diatomic dipole polarisabilities:

$$V_{pol}^{(o)}(R) = -\frac{\alpha_o(R)}{2r_e^4}; \quad \text{and}$$
$$V_{pol}^{(2)}(R) = -\frac{\alpha_2(R)}{2r_e^4} P_2[\cos(\hat{\mathbf{r}}_e \cdot \hat{\mathbf{R}})] \quad (13)$$

for the $H_2(R)$ the α_0 was varied over the range of internuclear distances that are relevant to the number of coupled asymptotic vibrational levels. At the equilibrium geometries our computed values were $\alpha_{xx} = 4.55a_o^3$ and $\alpha_{zz} = 6.31a_o^3$, to be compared with the experimental values [12] of $\alpha_{xx}^{expt} = 4.748a_o^3$ and $\alpha_{zz}^{expt} = 6.783a_o^3$. We have (somewhat arbitrary) scaled the radial dependence of the polarisability terms computed by us to reproduce the experimental values at R_{eq}, thus constructing a realistic long-range polarization potential over the required range of nuclear geometries to be included in the coupling integrals of equation (8).

One could, of course, employ better molecular wavefunctions in order to obtain from them better values for their dipole polarisabilities, However, since both short-range and long-range polarization effects are added to the interaction after the static potential is produced from the chosen target electronic density, we feel that one achieves the same result which could be given by a better basis set by simply scaling asymptotically the added correlation-polarization terms. The full SECP interaction was then rewritten using the familiar multipolar expansion in the Space-Frame (SF) reference system of its Jacobi coordinates

$$V_{SECP}(\mathbf{r}_{e'}|\mathbf{R}) = \sum_{L=0,\ even}^{L_{max}} V_L^{SECP}(r_e|R) P_L[\cos(\hat{\mathbf{r}}_e \cdot \hat{\mathbf{R}})] \quad (14)$$

The individual multipolar coefficients were then fitted with spline functions and the expansions extended up to the L_{max} values mentioned in Section 1. A pictorial example of the lowest multipolar coefficients ($L = 0$) for the H_2 molecule is shown in Figure 1, as a function of the internuclear values.

One clearly sees in both panels the presence of strong nuclear cusps associated to the nuclear attraction term in the static interaction. One further sees that the bond stretching motion markedly broadens the region of electron-molecule short-range interaction where the vibrational couplings are indeed acting the most strongly.

Such an effect is clearly exemplified by the calculations reported in Figure 2, where we have performed the convolution of the potential terms of Figure 1 over the vibrational wavefunctions of the $\nu = 0$ and $\nu = 1$ levels of H_2 calculated as described in the previous section.

It is interesting to see from the figure that the target deformation induced by the incoming electron is really highly localized within the short range region, where the target electronic cloud penetration by the impinging charge is the strongest: by the time the incoming projectile is beyond about $2.0a_0$ away from the target c.o.m., the strength of the coupling is seen to be reduced by nearly five orders of magnitude. Thus, we expect that a very low collision energies only the lower angular momenta will be able to access that region and significantly contribute to the excitation process.

Another interesting feature of the present interaction that is worth mentioning, as a numerical check of our calculations, could be gleaned from the results we present in Figure 3. What we report there is a comparison, for

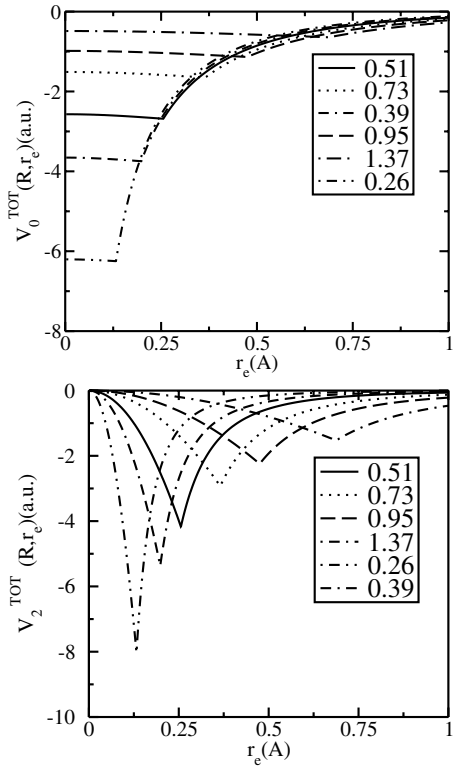

Fig. 1. Computed multipolar coefficients of the interaction in the short-range region from the molecular center-of-mass. Top panel: spherical multipolar terms; lower panel: $L = 2$ multipolar coefficients. The radial values in the panels report (in units of a_0) the distances of each H atom from the c.o.m.

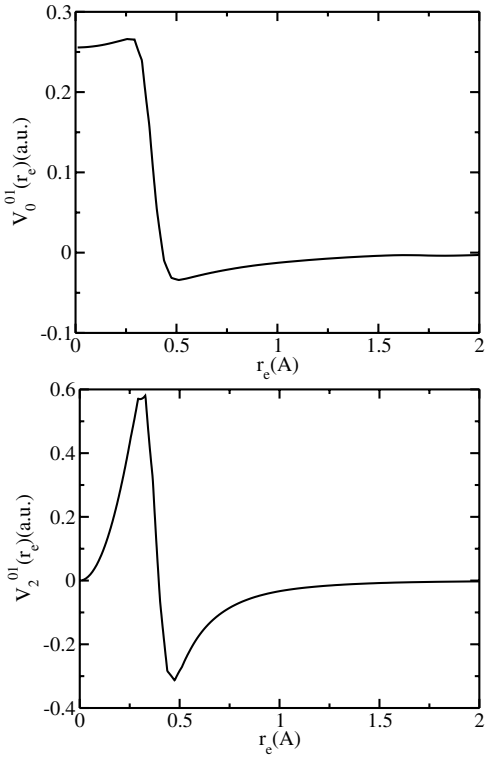

Fig. 2. Computed vibrational coupling matrix elements between $\nu = 0$ and $\nu = 1$ levels for the $L = 0$ and 2 multipolar potential terms. Upper panel: $V_0^{01}(r_e)$; lower panel $V_2^{01}(r_e)$. Distances in Å, energies in cm^{-1}.

the lowest two multipolar coupling potential terms, of the rigid-rotor interaction where the target molecule is kept at its equilibrium geometry, R_{eq}, (solid lines) and the diagonal coupling potential after convolution over the numerical ground state vibrational wavefunction, $\chi_0(R)$ (broken lines). We clearly see that the averaging reproduces very well the Rigid-Rotor interaction, indicating that in such a system the departure from anharmonicity at $\nu = 0$ is really rather small and therefore averages correctly to the potential where no distortion is being considered. The result also confirms the numerical reliability of both our computed wavefunctions and coupling vibrational potential terms.

Such analysis have been obviously carried out many times in the past (e.g. see Ref. [24]), but the present revisitation is solely meant to confirm the numerical reliability of the present approach and not its novelty of results: it simply serves us to establish the level of quality of the model potential employed in the present calculations in order to be able to extend its usage down to near-threshold energies, i.e. to processes induced by "cold" electrons.

3 The scattering results

3.1 "Tuning" the model exchange

As discussed in the previous section, we have modeled the all-important exchange interaction using a local form that

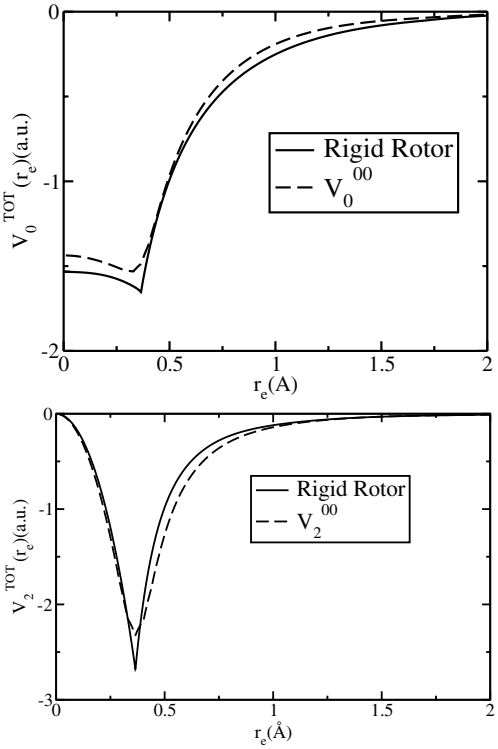

Fig. 3. Comparison of the lowest two multipolar coefficients of the interaction potentials obtained for the rigid rotor target (solid lines) and the adiabatic average over the ground vibrational state of H_2 (dashed lines).

has been used many times to simplify calculations [21]

$$V_{ex}^{HFEGE}(\mathbf{r}_e|\mathbf{R}) = \frac{2}{\alpha}k_F(\mathbf{r}_e)\left[\frac{1}{2}+\left(\frac{1-\eta^2}{4\eta}\right)\ln|\frac{1+\eta}{1-\eta}|\right] \quad (15)$$

where:

$$k_F(\mathbf{r}_e) = [3\pi^2\rho(\mathbf{r}_e)]^{1/2};$$
$$\eta(\mathbf{r}_e) = (k^2+2I_f+k_F^2)^{1/2}/k_F \quad (16)$$

the parameter appearing in the above model potential is the quantity I_f, the ionization potential of the target molecule. In the present case, the experimental I_f value is 0.56 a.u. [9]. Since we are therefore expected to know the I_f values over the range of internuclear distances that contribute to the vibrationally inelastic processes, and since we are not aware of any experimental determination of it for different molecular geometries (i.e. for vibrationally 'hot' targets), we decided to treat I_f as a "tuning" parameter for the elastic scattering process in calculations where the sum over the index $|f\rangle$ on the r.h.s. of Eq. (5) collapses to $f = |\nu_o\rangle$), making use of a comparison between such vibrationally elastic calculations and experiments that show rotational inelasticity only. In other words, we are "tuning" the I_f values by computing vibrationally elastic cross-sections for the target ground vibrational state. One should note here that, although this local modeling of the exchange potential is numerically convenient for an SF treatment of the dynamics, it does not reproduce accurately the scattering of electrons near the low-energy thresholds. Hence, we employ the above adjustable parameters to overcome such deficiencies and to obtain the best agreement with available vibrationally elastic cross-sections. This value of the I_f parameter is then used without further adjustment to study inelastic processes.

One first set of results are reported in Figure 4, where we show our computed elastic ($v = 0$, $j = 0 \rightarrow v' = 0$, $j = 0$) integral cross-sections (solid line) with the adjusted I_f value that best reproduced the reported experiments ($I_f = 0.24$ a.u.): one clearly sees that the overall agreement, at the energies considered, is rather good. The experimental data are over a large number of years and are listed in the caption of Figure 4.

In order to further test the efficiency of the "tuning" procedure and to be able to employ one single value at all geometries, we have further computed the rotationally inelastic partial cross-sections by using the required $V_L^{\nu\nu'}(r_e)$ potential coefficients in equation (5), as defined in equation (8). The results are shown in Figure 5, where we report in the upper panel the partial inelastic cross-section (solid line) for the ($j = 0 \rightarrow j' = 2$) excitation process in comparison with available experiments. The lower panel in the same figure reports the partial cross-sections for the ($j = 2 \rightarrow j' = 4$) inelastic cross-sections: both sets of calculations have used the same "tuned" value of I_f as that used for the calculations in Figure 4.

We see that both sets of calculations are reproducing the rotationally inelastic cross-sections reasonably well and thus we could use that value of I_f for the further calculations of the vibrationally inelastic cross-sections obtained as summed over all rotational excitations processes. The outcome of such calculations will be discussed in the following section.

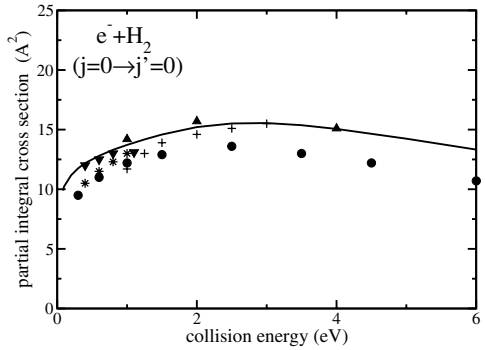

Fig. 4. Computed and measured integral elastic partial cross-sections ($v = 0$, $j = 0 \rightarrow v' = 0$, $j' = 0$) in comparison with existing experimental data: solid circles: from reference [24]; solid up triangles: from reference [25]; crosses: from reference [27]; stars: from reference [28]; solid down triangles: from reference [29].

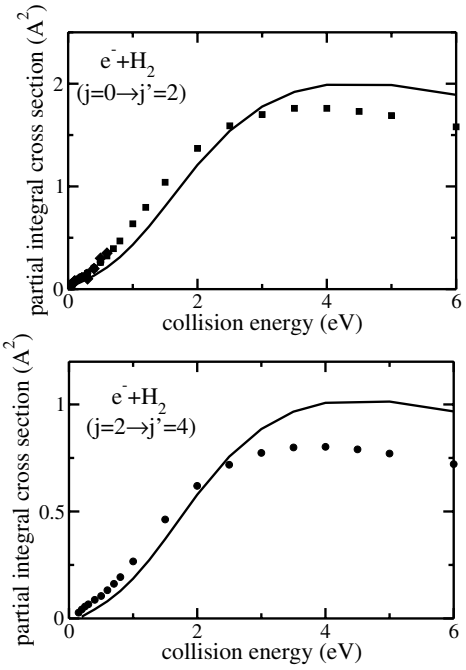

Fig. 5. Computed and measured partial, vibrationally elastic cross-sections for the (0→2) (upper panel) and the (2→4) (lower panel) rotational excitations of H_2 by electron impact. The experiments are, in the upper panel: filled circles from reference [30]; filled squares from reference [31]; filled lozenges from reference [32]. In the lower panel: filled circles from reference [32]. The vibrational state included was the $v = 0$ state only.

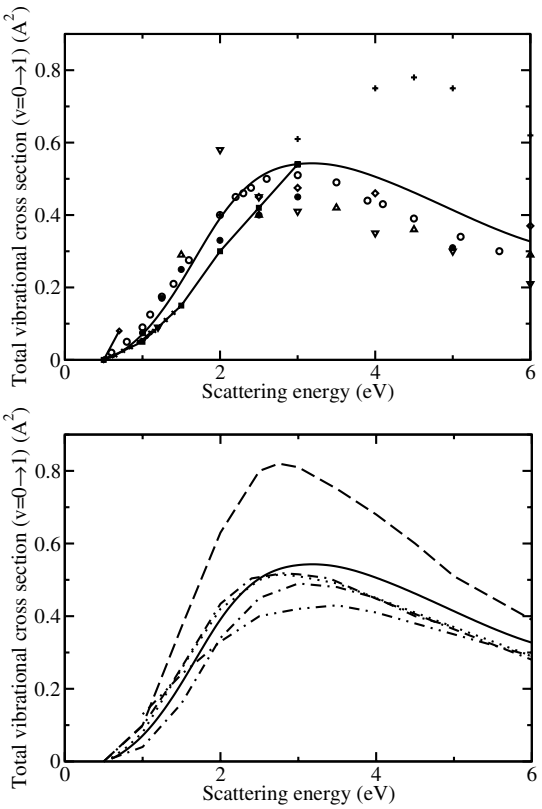

Fig. 6. Computed and measured partial inelastic cross-sections for the (0→1) vibrational excitation of H_2. The upper panel refers to the comparison of our present calculations (solid line) with the available experiments, while the lower panel compares present results (solid line) with other theoretical work. All the references are given below: filled circles = reference [37], open circles = reference [36], open triangles = reference [39], open diamonds = reference [40], lower triangles = reference [41], crosses = reference [31], filled diamonds = reference [43], filled squares = reference [42]. Lower panel: dots = reference [37], dot-dashes = reference [35], dash-dash-dots = reference [34], dot-dashes = reference [33], dot-dot-dashes = reference [44].

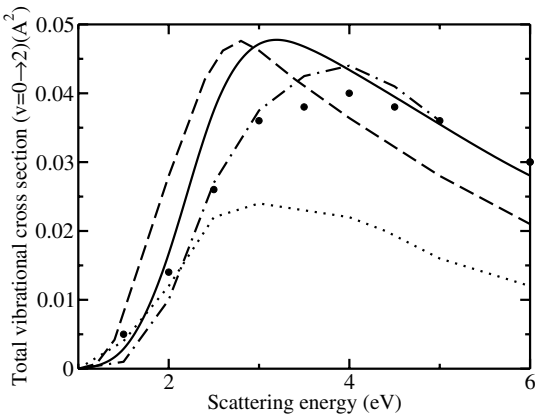

Fig. 7. Computed and measured vibrationally inelastic cross-sections for the (0→2) process. The solid line shows the present results while the dots refer to calculations from reference [44], the dashes are the calculations from reference [35] and the filled circles are experiments from reference [36]. The dot-dashed results are calculations from reference [33].

3.2 The vibrationally inelastic cross-sections

There have been several experimental measurements on the $e^- - H_2$ vibrational excitation processes, as well as theoretical evaluations by several authors. In Figure 6 we report in the top panel the inelastic partial cross-sections for the ($\nu = 0 \rightarrow 1$) excitation in comparison with the experimental data (the corresponding references are given in the figure caption). The present calculations are indeed following the experiments very closely over the whole range of energies and appear to perform very well at those low energies above threshold where adiabatic methods are usually failing.

It is certainly reassuring to see how well the present calculations are able to reproduce experiments and also earlier calculations for that transition process. A similar comparison for the (0→2) excitation cross-section is reported by Figure 7, where only one experimental evaluation has been found. Our calculations (solid line) are doing again rather well, especially close to threshold and up to about 2 eV above it. One sees however that our computed values are larger than experiments around the broad resonance and match them again very well beyond the latter. In general, we see that the delicate region at threshold is well reproduced by the present, exact calculations with a model potential. As one enters the broad resonance region, around 4 eV, however, one sees that our computed values increase with energy faster than the experiments and peak at a lower energy than the latter data. Such a discrepancy could be due to the use of a model exchange interaction since we are probing that collision energy range where the exciting electron begins to penetrate more deeply the target charge distribution and therefore the "tail" features of an essentially short-range interaction like exchange become important. It is still reassuring, however, to see that both the (0→1) and (0→2) excitation cross-sections obtained here follow closely existing experiments and earlier calculations. For simplicity of presentation, we have omitted to explicitly report the calculations of Lee and Mazon [45], which coincide with the results (quoted in Fig. 6) of reference [33], and the earlier experimental data of Allan of reference [46].

In order to numerically test the level of convergence that we have achieved with the present calculations, we report in Table 1 the results for such tests. We show there, in the top panel, the vibrationally elastic (rotationally summed) cross-section values as a function of $V_{\lambda max}$, the highest multipolar term included in the interaction potential of equation (8). The next panel below the latter shows the numerical convergence of the same type of the elastic cross-sections as a function of the number of rotational states included by the Coupled Channel expansion of the scattering equations (5), while the third panel below the latter is reporting the same convergence test but on the number of vibrational states being included by the CC expansion. Finally, the last panel at the bottom of the table shows the convergence efficiency on the inelastic processes,

Table 1. Computed vibrational cross-sections as a function of selected convergence parameters (all values in Å^2). The results are shown at two different energies: E_1(=1.0 meV) and E_2(=6.0 eV).

E_1		E_2	
$V_{\lambda max}$	$\sigma(0 \to 0)$	$V_{\lambda max}$	$\sigma(0 \to 0)$
1	11.880	1	13.728
2	8.528	2	13.752
3	8.009	3	13.718
4	7.887	4	13.711
5	7.887	5	13.709
6	7.861	6	13.707
7	7.834	7	13.707
8	7.823	8	13.706
9	7.825	9	13.705
10	7.820	10	13.704
j_{max}	$\sigma(0 \to 0)$	j_{max}	$\sigma(0 \to 0)$
2	8.376	2	13.857
4	7.964	4	13.726
6	7.872	6	13.744
8	7.840	8	13.714
10	7.832	10	13.699
12	7.826	12	13.708
14	7.820	14	13.707
16	7.818	16	13.706
18	7.820	18	13.704
ν_{max}	$\sigma(0 \to 0)$	ν_{max}	$\sigma(0 \to 0)$
1	7.818	1	13.706
2	7.485	2	13.609
3	7.567	3	13.325
4	7.555	4	13.321
ν_{max}	$\sigma(1 \to 0)$	ν_{max}	$\sigma(0 \to 1)$
2	2.858	2	0.0853
3	2.745	3	0.3227
4	2.748	4	0.3232

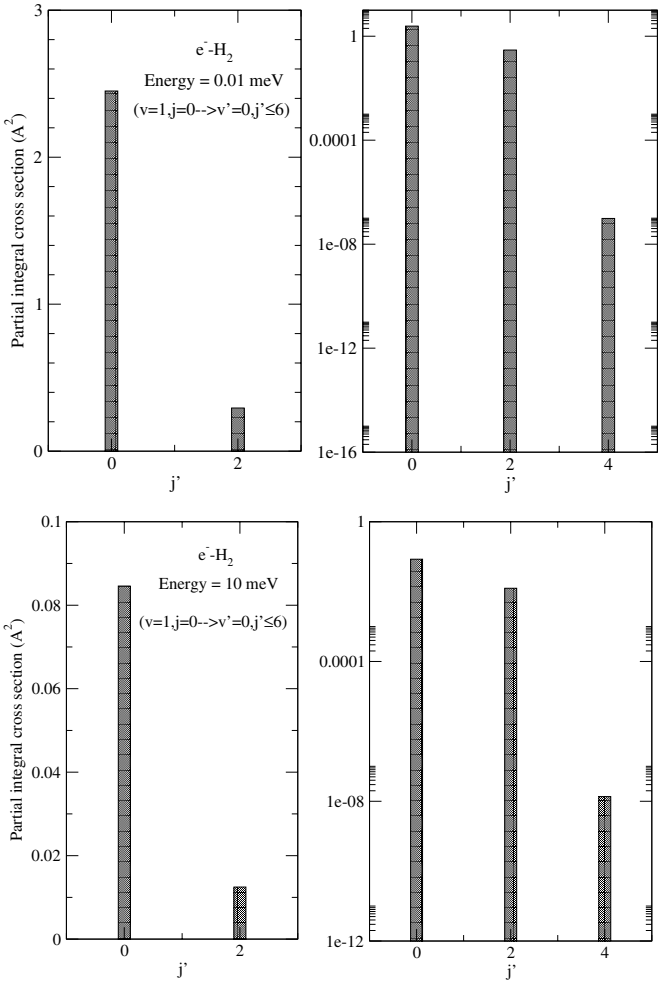

Fig. 8. Computed vibrational superelastic cross-sections between the $|v = 1, j = 0\rangle$ and $|v' = 0, j'\rangle$ levels of H_2 at two different collision energies. See text for details.

$\sigma(1 \to 0)$ and $\sigma(0 \to 1)$, respectively. The latter quantities also correspond to rotationally summed results. It is clear from the data in the table that our level of convergence (shown for two energy values but actually tested by us for many more energies) is better than 0.1% for the cases examined.

3.3 The very-low energy inelastic processes

As mentioned in the foregoing discussion, the above calculations over the energy range we have examined do not necessarily require the further complication of using an SF representation of the dynamics, a point often discussed in the existing literature (e.g. see Ref. [24]). However, when one needs to move down in energy and close to the threshold openings then the correct dynamical frame needs to be employed. Thus the use of the full coupled-channel treatment for the results of the previous section was chiefly meant as a test of the reliability of the present approach. Its extension down to the meV range, however, has as a mandatory requirement the use of the correct SF angular momentum coupling that we have implemented in the present analysis.

The interest in "cold" electrons dynamics has markedly increased in recent years, due to a variety of experiments on molecular gas [47,48] and therefore any theoretical study of inelastic processes at such low energies requires SF dynamics.

As an example of what can be obtained with a fully converged calculation, we report in Figure 8 the behavior of the superelastic collisions for the vibrationally excited ($v = 1$) molecular target as a function of the final rotational level, having assumed to start in the $|v = 1, j = 0\rangle$ rotovibrational H_2 state. Two different collision energies are given in the panels: 10 μeV in the upper panels and 10 meV in the lower panel. The results shown by Figure 9 refer to the same type of processes by starting with the molecule in its $|v = 1, j = 10\rangle$ state.

The upper left panels report the largest collisional superelastic cross-sections, i.e. the Δj=0 process, plus the ones where partial rotational excitation occurs into the next level, while the right upper panels reports, on a log

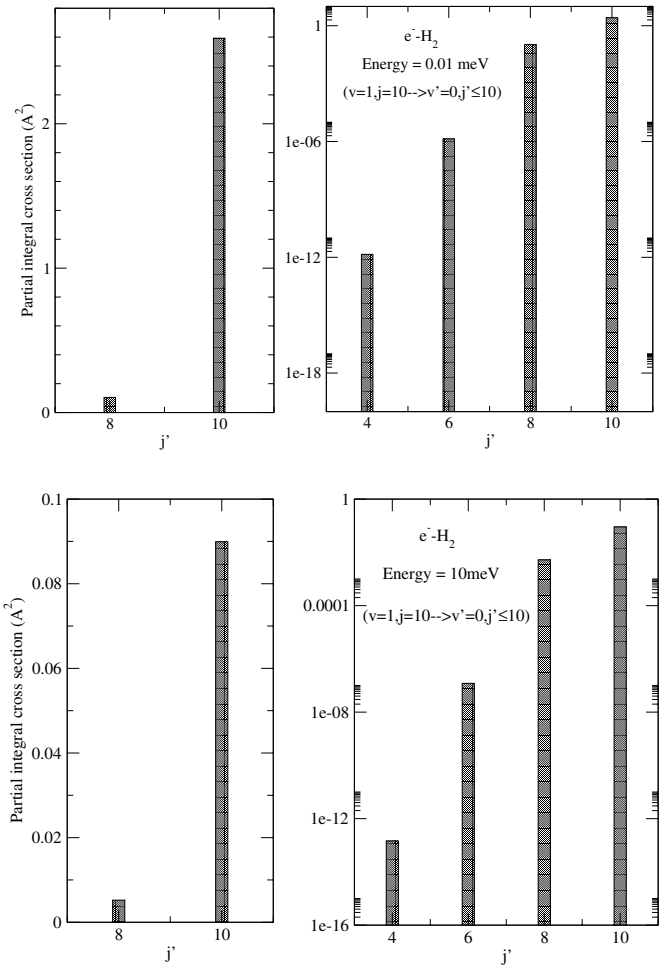

Fig. 9. Same as in Figure 8 but for the target molecule chosen to be in the $|v = 0, j = 10\rangle$ initial state.

scale, also the other partial cross-sections into a higher j' values.

One clearly sees from the figures that the $\Delta j = 0$ and $\Delta j = +2$ cross-sections dominate the spectrum while the other cross-section is orders of magnitude smaller and the higher j' ones are not even visible in the figure. Furthermore, over the energy changing of three orders of magnitude between upper and lower panels in each figure the corresponding cross-sections are also quite different and appear to be getting closer to following the linear Wigner's regime [49] of exponential increase with decreasing collision energy already observed by us with ionic partners [50]. We also see that even at the lowest energies considered the inelastic processes still remain sizeable in spite of the expected inefficiency of the light electron to excite vibrations in a strong bond like that of H_2. This finding should be important for the analysis of the size of the observed total cross-section as the collision energies go to zero. We shall discuss further aspects of the very-low energy regimes in our work currently in preparation [49].

4 Present conclusions

In this work we have revisited the computation of vibrationally inelastic, partial integral cross-sections of gaseous H_2 by collision with slow electrons, examining the range of energies from thresholds up to a few eV above them. The quantum treatment of the dynamics has been carried out entirely in the laboratory reference frame and the coupled-channel equations were employed with a rigorous inclusion of all the rotovibrational target states required to reach convergence of cross-section values around 10^{-5}. The interaction forces have been modelled in local form and the exchange interaction has been included via the Hara's FEGE model [19]. In order to describe the dependence of such a model on the internuclear motion during the excitation process, we have treated the I_f parameter of equation (16) as a disposable quantity, adjusting it to reproduce the vibrationally *elastic* cross-sections (rotationally elastic and inelastic) given by experiments. The value obtained has then been employed to treat vibrational inelasticity, producing final cross-sections in excellent accord with existing experiments.

Given the complexity of solving a large number of coupled equations, we feel that our present Modified Variable Phase Approximation [11] provides a robust computational tool that allows us to reach convergent cross-sections with a marked reduction of computational time.

The method has been further shown by the present numerical "experiments" to be able to describe well electron collisions on H_2 that cause rotovibrational excitations of the target in the energy regions where experiments exist. Thus, we feel our present modelling of the interaction forces could also be profitably extended to other diatomics by using similar forms of the forces at play [41,42].

As a preliminary example, we have shown the behavior of the de-excitation cross-sections as a function of final rotational state and for two, very low collision energies.

We therefore think that the SF approach should be the method of choice for generating quantum inelastic cross-sections at very low energies which are close to their relevant thresholds and which do play a very important role for the interpretation of the variety experiments carried out with cold electron beams [51,52] Such quantities also involve nonlinear polyatomic gases, a rather straightforward extension within our present computational scheme, and are of further interest when the considered collision energies go down to the μeV range, thus becoming relevant for the study of molecular collisions in cold traps [53]: all such extensions of the present work are rather simple ones in terms of computational modifications of our present quantum code and will be the object of future studies [54].

The financial support of the Research Committee of the University of Rome "La Sapienza", of the CASPUR Supercomputing Center and of the EPIC EU Research Training Network are gratefully acknowledged. One of us (S.T.) further thanks the EPIC Network (HPRN-CT-2002-00179) for the award of a Research Fellowship to the University of Rome during the year 2003.

References

1. e.g. see: *Adv. At. Mol. Opt. Phys.,* edited by B. Bederson, H. Walthers (Academic Press, New York, 1994)
2. *Electron Molecule Collisions*, edited by I. Shimamura, K. Takayanagi (Plenum Press, New York, 1994)
3. *Electron Collisions with Molecules, Clusters, Surfaces*, edited by H. Ehrhardt, L.A. Morgan (Plenum Press, New York, 1994)
4. S. Trajman, D.F. Register, A. Chutjian, Phys. Rep. **97**, 219 (1983)
5. A. Zecca, G.P. Karwasz, R.S. Brusa, Nuovo Cim. **19**, 1 (1996)
6. e.g. see: *Computational Methods for Electron-Molecule Collisions*, edited by W.M. Huo, F.A. Gianturco (Plenum Press, New York, 1995)
7. J.W. Mc Conkey, S. Trajmar, G.C.M. King, Comm. At. Mol. Phys. **22**, 17 (1988)
8. H. Tawara, I. Ytikawa, H. Nishimura, M. Yoshino, J. Phys. Chem. Res. Data **19**, 617 (1990)
9. M.A. Morrison, R.W. Crompton, B.C. Saha, Z.L. Petrovic, Aust. J. Phys. **40**, 239 (1987)
10. M.J. Brunger, S.J. Buckman, Phys. Rep. **357**, 215 (2002)
11. D. Field, S.L. Lunt, J.-P. Ziesel, Acc. Chem. Res. **34**, 2186 (1999)
12. D. Field, C.N. Jones, S.L. Lunt, J.-P. Ziesel, Phys. Rev. A **60**, 291 (2001)
13. E. Bodo, R. Martinazzo, F.A. Gianturco, Comp. Phys. Comm. **151**, 187 (2003)
14. F. Calogero, *Variable Phase Approach to Potential Scattering* (Academic, New York, 1967)
15. R.J. Le Roy, Level 7.2, Chem. Phys. Res. Rep., CP-555R (2000)
16. e.g. see: F.A. Gianturco, A. Jain, Phys. Rev. **143**, 347 (1986)
17. F.A. Gianturco, R.R. Lucchese, N. Sanna, J. Chem. Phys. **100**, 6464 (1994)
18. R. Curik, F.A. Gianturco, J. Phys. B **35**, 1235 (2002)
19. R. Curik, F.A. Gianturco, N. Sanna, Int. J. Quant. Chem. **84**, 565 (2001)
20. F.A. Gianturco, Ga. Kashenok, R.R. Lucchese, N. Sanna, J. Chem. Phys. **116**, 2811 (2002)
21. S. Hara, J. Phys. Soc. Jpn **22**, 710 (1967)
22. F.A. Gianturco, J.A. Rodriguez-Ruiz, A. Jain, Phys. Rev. A **48**, 4321 (1993)
23. F.A. Gianturco, A. Jain, L. Pantano, J. Phys. B **20**, 571 (1987)
24. M.A. Morrison, Adv. At. Mol. Phys. **24**, 51 (1988)
25. I. Shimamura, Sc. Pap. Inst. Phys. Chem. Res. **82**, 1 (1989)
26. J. Furst, M. Maghereften, D. Golden, Phys. Rev. A **30**, 2256 (1984)
27. M.J. Bruger, S.J. Buckman, D.S. Newman, D.T. Alle, J. Phys. B **24**, 1435 (1991)
28. E. Golden, H.W. Bandel, J.A. Salerno, Phys. Rev. **146**, 40 (1966)
29. C. Ramsauer, R. Kollath, Ann. Phys. **4**, 91 (1929)
30. A.G. Robertson, M.T. Elford, R.W. Crompton, M.A. Morrison, W. Sun, W.K. Trail, Aust. J. Phys. **50**, 441 (1997)
31. A.G. Engelhard, A.V. Phelps, Phys. Rev. **131**, 2115 (1963)
32. A.G. Engelhard, L.P. Elford, R.W. Crompton, J. Phys. B **61**, 573 (1988)
33. H. Gao, Phys. Rev. A **45**, 6895 (1992)
34. R.J.W. Henry, Phys. Rev. A **2**, 1349 (1970)
35. S. Mazevet, M.A. Morrison, O. Boydstun, R.K. Nesbet, Phys. Rev. B **32**, 1269 (1999)
36. H. Ehrhardt, L. Langhans, F. Linder, H.S. Taylor, Phys. Rev. **173**, 222 (1968)
37. S.J. Buckman, M.J. Brunger, D.S. Newman, G. Snitchler, S. Alton, D.W. Norcross, M.A. Morrison, B.C. Saha, G. Danby, W.K. Trail, Phys. Rev. Lett. **65**, 3253 (1990)
38. J.P. England, M.T. Elford, R.W. Crompton, Austr. J. Phys. **41**, 573 (1988)
39. F. Linder, H. Schmidt, Naturforsch. **26a**, 1603 (1971)
40. N. Nishimura, A. Danjo, H. Sugahara, J. Phys. Soc. Jpb **54**, 1757 (1985)
41. G.J. Schultz, Phys. Rev. **135**, 988 (1964)
42. R.W. Crompton, D.K. Gibson, A.G. Robertson, Phys. Rev. A **2**, 1386 (1970)
43. P.D. Burrow, G.J. Schultz, Phys. Rev. **187**, 97 (1969)
44. R.J.W. Henry, E.S. Chang, Phys. Rev. A **5**, 276 (1972)
45. M.T. Lee, K.T. Mazon, Phys. Rev. A **65**, 042720 (2002)
46. M. Allan, J. Phys. B **18**, L451 (1985)
47. D. Field, N.C. Jones, J.-P. Ziesel, Phys. Rev. A **69**, 052716 (2004)
48. N.C. Jones, D. Field, J.-P. Ziesel, T.A. Field, J. Chem. Phys. **122**, 07431 (2005)
49. E.P. Wigner, Phys. Rev. **72**, 1002 (1948)
50. E. Bodo, F. Sebastianelli, E. Scifoni, F.A. Gianturco, A. Dalgarno, Phys. Rev. Lett. **89**, 283201 (2002)
51. D. Field, J.-P. Ziesel, S.L. Lunt, R. Parthasarathy, L. Suess, S.B. Hill, F.B. Dunning, R.R. Lucchese, F.A. Gianturco, J. Phys. B **34**, 4371 (2001)
52. D. Field, N.C. Jones, S.L. Lunt, J.-P. Ziesel, Phys. Rev. A **64**, 22708 (2001)
53. e.g. see: P. Pellegrini, O. Dulieu, F. Masnou-Seeuws, Eur. Phys. J. D **20**, 77 (2002)
54. S. Telega, F.A. Gianturco, in preparation